

A FARM OF WAVE ACTIVATED BODIES FOR COASTAL PROTECTION PURPOSES

Angelelli E.¹ and Zanuttigh B.²

This paper aims at investigating the efficacy of a floating farm of wave energy converters for coastal protection purposes through physical and numerical modelling. The experiments were performed in 3D conditions on a basic module consisting of two staggered lines and three devices. The numerical simulations were carried out with the software MIKE 21 BW, developed by DHI Water & Environment & Health, and were calibrated based on the experimental results. Additional configurations were tested by varying the gap long-shore width and the device alignment. Despite the model limitations, i.e. the representation of the devices as fixed porous piles, the numerical results well approximate the average measured transmission coefficient and allow to derive a complete map of the hydrodynamics around the devices.

Keywords: floating wave farm, MIKE 21 BW, numerical model, calibration, experiments

1- INTRODUCTION

Coastal defence in a changing climate poses new challenges (Nicholls and de la Vega-Leinert, 2008). Defence solutions should be climate-proof and at the same time economically feasible while preserving the coastal ecosystem (Zanuttigh, 2011).

Floating breakwaters are characterized by the adaptability to sea level rise, by limited aesthetic and environmental impact and are usually deployed under mild climate. If floating structures are combined with a power extraction system, i.e. Wave Energy Converters (WECs), these solutions become more efficient in absorbing incident wave energy and more attractive in terms of multi-purpose installation.

The combination of wave energy production and coastal protection is actually rather innovative, being usually examined the impact of off-shore WEC installation for EIA purposes instead of designing such installation for producing a given impact on the littoral.

Few studies are available in the literature on the hydrodynamic performance of wave farms. Most of the literature deals with the efficiency and stability of single WEC, based on experiments or simulations. Numerical simulations are essentially performed with two main objectives: the refraction-diffraction analysis around the devices and the estimation of the impact on the shoreline. For the first purpose, the numerical codes usually adopted are based on the linear theory, neglect viscous dissipation and solve the governing equations based on the Boundary Element Method (Cruz et al., 2009). For the latter case the devices (or wind piles) are typically represented through an equivalent bottom friction or percentage of wave energy absorption with 2D or quasi 3D codes (Palha et al., 2010).

Objectives of this paper are

- to examine the hydrodynamics around a farm of multiple floating WECs, with specific focus on wave transmission;
- to investigate the sensitivity of such devices to climate change by varying water depth at installation;
- to assess the interactions among the devices and therefore provide design guidelines for the optimal layout of the wave farm.

To achieve these objectives, the investigation was preliminarily carried out in the wave basin at Aalborg University, where a basic wave farm staggered module was tested under a variety of wave attacks, accounting for sea level rise variation. The paper first presents the experimental set-up and synthesizes the most relevant results in terms of wave transmission coefficients behind the devices and wave heights at the gap. To extend the experimental database, numerical simulations were performed with Mike 21 BW, following an approach similar to the work on the Wave Dragon by Beels et al. (2010). The paper first describes the model set-up, the representation of the floating bodies by means of fixed porous layers and the model calibration. Different farm configurations are then analysed, specifically changing the device alignment and mutual distance. Some conclusions regarding the device and farm layout are finally drawn.

¹ DICAM, University of Bologna, Viale Risorgimento 2, Bologna, 40136, Italy
elisa.angelelli4@unibo.it

² DICAM, University of Bologna, Viale Risorgimento 2, Bologna, 40136, Italy
barbara.zanuttigh@unibo.it

2- EXPERIMENTAL SETUP AND MAIN RESULTS

2.1- Device and Farm description

The floating WEC under investigation is called DEXA (www.dexawave.com) and it belongs to the Wave Activated Bodies typology (WAB). Two rigid pontoons with a hinge in between compose the body of the device (see Fig. 1). The device is inspired to the Cockerell principle, optimizing it through a redistribution of buoyancy and force at the extremity of the pontoon (Wheeler, 2001). At the steady state the free water surface passes in correspondence of the axis of the pontoons. The rotation of each pontoon, in relation to the other, causes the activation of the Power Take-Off (PTO) system. The PTO consists of a low pressure power transmission technology (Kofoed, 2009).

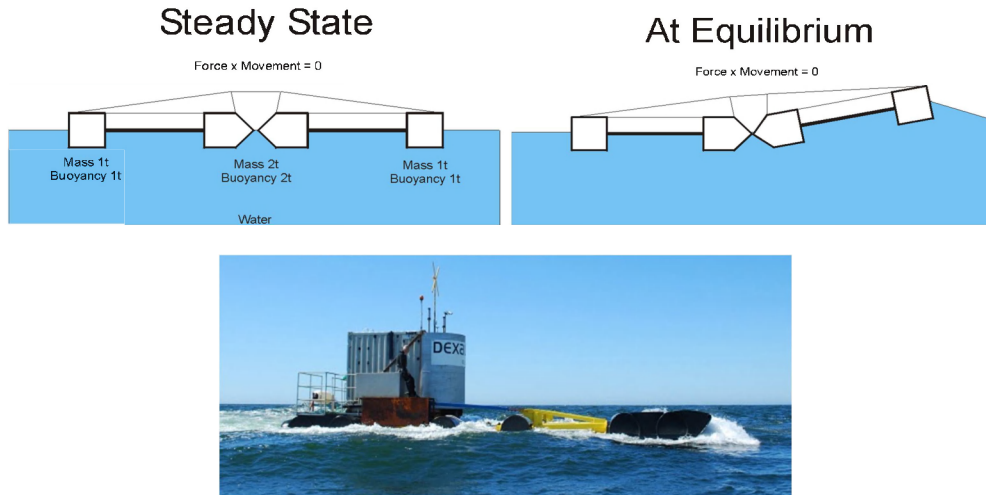


Figure 1. Scheme of the DEXA operational concept and picture of the 1:5 installation in Hantsholm, DK.

Three devices, in 1:60 scale, were adopted to represent a basic module of the WECs farm. Each device is 0.96m long in the cross-shore direction (dimension in the following indicated as l) and 0.38m wide (b). The initial configuration (see Fig. 2) has the three devices in a staggered position, i.e. two in the first line and one in the second line at the center of the first gap line. The gap width is approximately $8b$, while the cross-shore distance among the devices is about $2l$.

2.2- Facility and measurements

The devices were tested in the directional deep wave basin of the Hydraulics and Coastal Engineering Laboratory at Aalborg University, DK. The basin is 15.7 m long (in waves direction), 8.5 m wide. The bottom is made of concrete and characterized by a constant depth, while the inshore part consists of a 1:4 slope dissipative beach of sea stones.

The wave farm module was subjected to several wave states (WSs), in order to describe the effects of changes in wave period T_p , wave height H_s and water depths (see Tab. 1). These WSs correspond to 3D Jonswap irregular non-breaking waves, at intermediate depth condition (being $1/20 < h_{max}/L_0 < 1/2$). Table 1 reports also the ratio l/L_p , where L_p is the peak wave length.

Table 1. Wave States, where H_s is the significant incident wave height, T_p is the peak wave period, L_p is the peak wave length and l is the device length; values are in full scale.				
WS	H_s [m]	T_p [s]	L_p [m]	l/L_p
1	3.00	5.7	49.7	1.20
2	3.00	6.5	62.8	1.00
3	3.00	7.8	83.3	0.75
4	3.00	10.6	125.7	0.50
5	4.00	7.8	83.3	0.75
6	4.00	10.6	125.7	0.50
7	5.00	7.8	83.3	0.75
8	5.00	10.6	125.7	0.50

Each test had a duration of 30 minutes, and it was repeated for two water depths: 0.30m and 0.35m. The hydrodynamic measurements were performed by using a total number of 27 resistive Wave Gauges (WGs), which give the instantaneous value of the surface elevation (see Fig. 2).

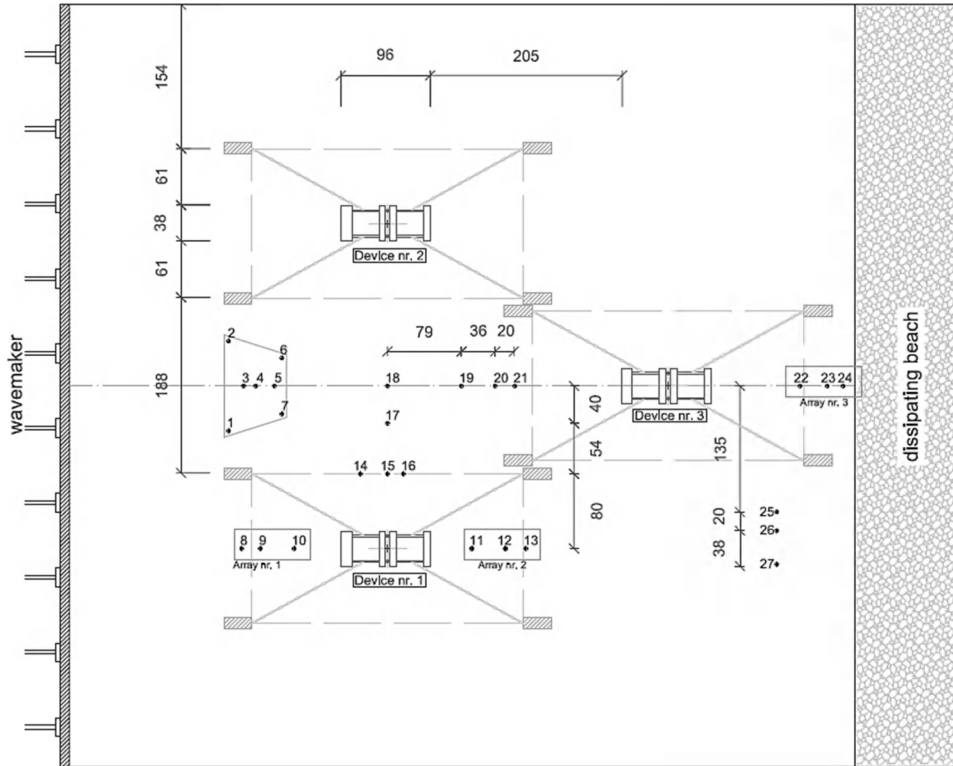


Figure 2. Laboratory overview with the three devices in a staggered configuration with the 27 WGs.

2.3- Main experimental results: wave transmission and wave interaction

To evaluate the behavior of the wave farm for coastal protection purposes, the wave transmission and the wave interaction are selected as key results. Further results on the experimental activity are available in Zanuttigh et. al. (2011).

Figure 3 reports the wave transmission coefficient for the front device (K_{T1} , derived from the ratio of H_s at the WGs 11-13 and WGs 8-10) and for the back device (K_{T3} , derived from the ratio of H_s at the WGs 22-24 and WGs 8-10) for the two water depths at installation. It can be observed that K_T decreases with increasing l/L_p , whereas the water depth h seems not to significantly affect K_T . It can be appreciated the lower values of K_{T3} with respect to K_{T1} suggesting that the third device is placed in a sheltered area induced by the wave interaction with the two devices in the first line.

The values, in full scale, of the wave height in the gap are summarized in table 2. The long-shore wave interaction can be stated from the measurements at the WGs 15-17-18, leading to an increasing of H_s from the device of the first line to the center of the gap. The cross-shore wave interaction is derived from WGs 18-19-20-21, leading to a decreasing of H_s from the center of the gap toward the device of the second line.

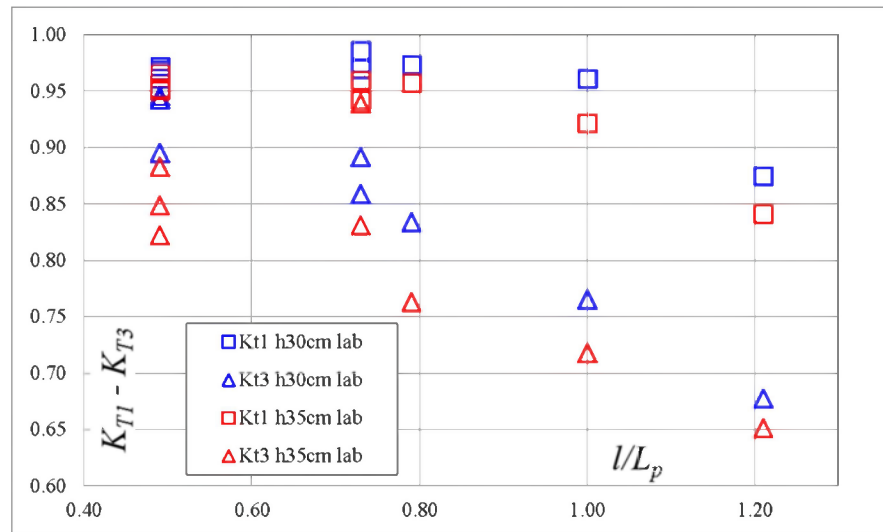


Figure 3. K_T from the laboratory data, for the two water depths.

WS	H_s WG15 [m]	H_s WG17 [m]	H_s WG18 [m]	H_s WG19 [m]	H_s WG20 [m]	H_s WG21 [m]
1	1.55	1.41	1.43	1.40	1.37	1.37
2	1.74	1.66	1.77	1.55	1.49	1.51
3	1.80	1.91	1.97	1.84	1.70	1.70
4	1.99	1.96	2.42	2.23	2.10	2.07
5	2.36	2.38	2.54	2.80	2.61	2.56
6	2.59	2.78	2.98	3.05	2.82	2.82
7	3.04	3.24	3.41	3.31	3.10	3.09
8	3.55	3.72	3.87	3.91	3.65	3.63

3- NUMERICAL MODEL SETUP

3.1- Model Description

The software MIKE 21 BW has been chosen to carry out the numerical simulations. MIKE 21, developed by DHI Water & Environment & Health (user guide and scientific documentation, 2008) is a modeling system for 2D free-surface flows, such as e.g. estuaries, coastal waters and seas.

MIKE 21 BW, i.e. the Boussinesq Wave module, is the model for calculation and analysis of short- and long-period waves in ports and coastal areas. This model is based on the numerical solution of the enhanced Boussinesq equations formulated by Madsen and Sørensen (1992) and their updates related to the representation of wave breaking and moving shoreline. MIKE 21 BW is able to reproduce the combined effects of wave phenomena, such as shoaling, diffraction, partial reflection and transmission from obstacles and internal wave generation (including directional spreading).

3.2- Model Set-up

The hydrodynamics induced by the WEC farm is represented with the 2DH BW module. The numerical domain corresponds to an extended version of the wave basin, to avoid side effects. A high-resolution rectangular grid (grid spacing 0.05m) is selected. The simulations are carried out with classical Boussinesq equations, by imposing wave absorption and measured water levels or target Jonswap wave spectrum at the off-shore boundary. An appropriate 50 lines sponge layer is set behind the numerical wave maker. The beach is represented as impermeable in the first tests and as a porous layer after in depth analysis and model calibration.

As described in Angelelli et. al. (2012), the three floating devices are reproduced as porous layers whose value (so called porous factor) has been derived from an iterative procedure, i.e. by calibrating numerical and experimental wave transmission and reflection coefficients.

The simulated surface elevations in time are extracted in correspondence of the same 27 positions of the laboratory WGs, to evaluate the significant wave heights both in time and frequency domain.

The first validation of the model set-up is centred on the wave energy comparison at the wave maker. A good approximation of the incident wave energy spectrum and an overestimation of the reflected wave energy was found in Angelelli et. al. (2012), both when wave generation was forced with the measured water levels and when the target Jonswap wave spectrum was selected. A possible solution for reducing wave reflection may be a different representation of the beach dissipation in the model. The analysis was however limited to the frequency-energy distribution; a thorough study has been then performed, including also the wave energy directional analysis. Figure 4 reports the comparison among experimental and numerical wave energy spectrum –both in frequency and direction- for WS6. In several WSs, the spectrum has a greater spreading factor in the lab than in the numerical simulations, both in frequency and direction. As it will be shown later on the approximation of measured and simulated wave transmission was overall good; however a different spreading could lead to a different wave height distribution in the wake of the devices and therefore would be worthy of further investigation for a more accurate representation of wave transmission.

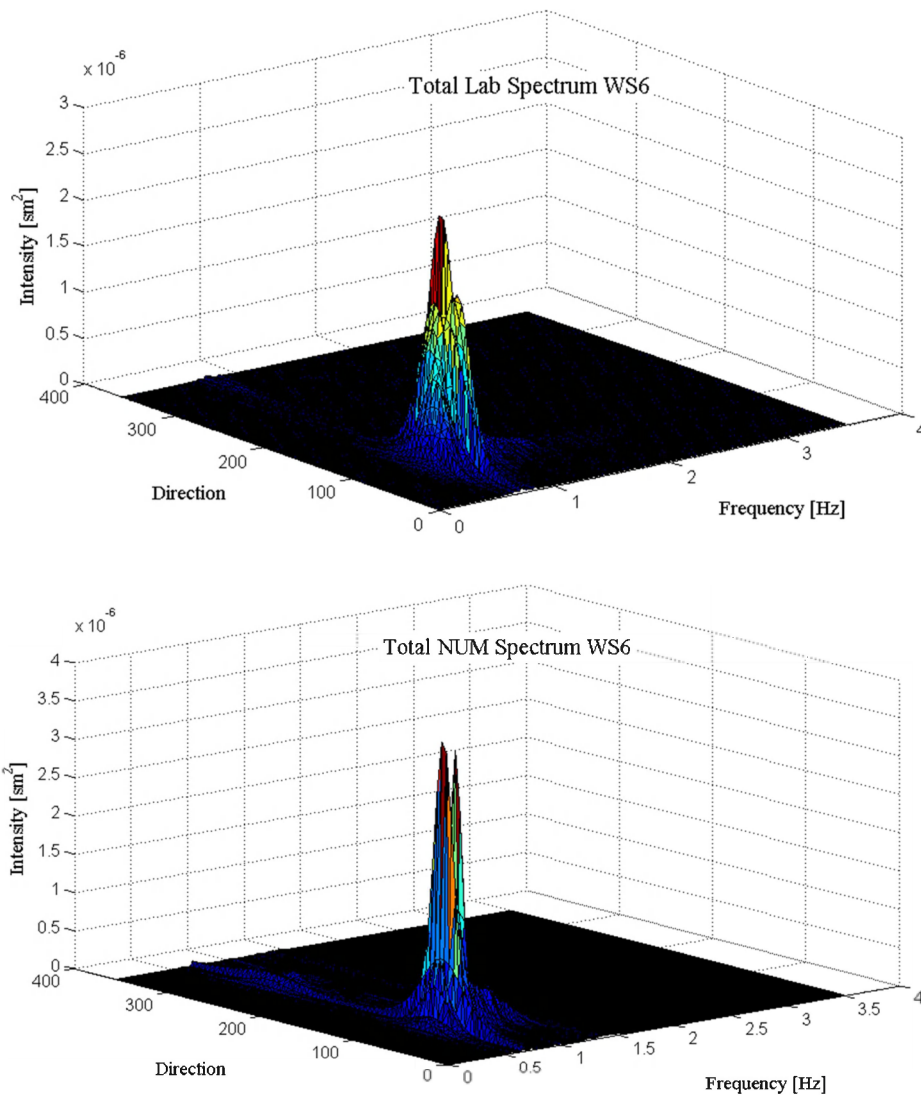


Figure 4. 3D Wave energy spectrum for the WS n.6 for the laboratory tests (on the top) and for the numerical simulations (on the bottom).

3.3- Numerical Result from the calibration

Numerical and experimental values of H_s are in good agreement over all the basin but differ at the gap where the numerical values are almost constant. This discrepancy can be explained with the device motion, since in the numerical simulation the device is modelled as a fixed body (a porous pile with rectangular section). For an easier comprehension figure 5 shows, to the left, the comparison of experimental and numerical H_s for WS 4 -5 - 7 and a zoomed plot of the long-shore WGs in the gap to the right.

The K_T induced by the single devices is well reproduced by the simulations as presented in table 3, differing the average values for less than the 3.5% for K_{T1} and 7% for K_{T3} (e.g. in case the water depth equals 0.30m). This agreement is found for a porous factor of 0.9 that is kept constant for all WSs (Angelelli et. al., 2012).

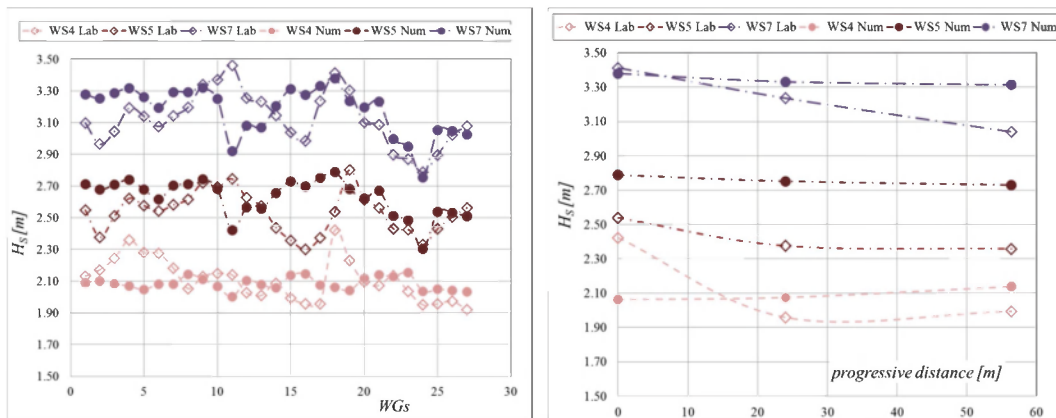


Figure 5. Wave height in the 27 WGs for the laboratory and the numerical simulation to the left, and of the long-shore WGs of the gap to the right, for the WS 4-5-7.

WS	$h_1 = 0.30$ m				$h_2 = 0.35$ m			
	$K_{T1,LAB}$	$K_{T1,NUM}$	$K_{T3,LAB}$	$K_{T3,NUM}$	$K_{T1,LAB}$	$K_{T1,NUM}$	$K_{T3,LAB}$	$K_{T3,NUM}$
1	0.88	0.82	0.68	0.82	0.84	-	0.84	-
2	0.96	0.90	0.77	0.86	0.92	-	0.92	-
3	0.97	0.94	0.83	0.92	0.96	0.94	0.96	0.94
4	0.97	0.97	0.95	0.96	0.95	0.98	0.95	0.97
5	0.97	0.93	0.89	0.90	0.94	0.93	0.94	0.92
6	0.97	0.96	0.94	0.94	0.97	0.96	0.97	0.95
7	0.99	0.92	0.86	0.89	0.96	0.92	0.96	0.91
8	0.96	0.95	0.90	0.92	0.95	0.95	0.95	0.93

In order to represent the wave transmission behind the lines of a wave farm, simplified assumptions were made when dealing with local measurements only. To obtain the value of K_{T2} , i.e. the average value of K_T behind the first farm line, a weighted average was calculated considering constant the values of K_{T1} for the space occupied by the device and its anchors, and a value equal to 1.00, i.e. total transmission, for the remaining basin zones. K_{T4} , i.e. the average value of K_T behind the second farm line, is derived in a similar way, by replacing the value of K_{T3} in the space in between the anchors of the third device. The approximation to keep constant the transmission coefficient for a long-shore reach that equals the space between the anchors was based on the measured trend of H_s at WGs 22-25-26-27 (Zanuttigh et. al., 2011).

In order to check these assumptions, numerical results are extracted along two long-shore lines (covering the whole long-shore extension of the experimental tank) corresponding to the measurement points (WGs 12 and 22). Figure 6 shows for WS 2 a good match among the laboratory trend -derived from the local measurements and the approximation synthesized above- and the grid by grid values of

wave transmission derived from the simulations. Both the effects of wave interaction at the gap (values greater than 1) and the reduction of wave height induced by the devices can be appreciated.

Furthermore, figure 7 compares the lab and numerical values of K_{T2} and K_{T4} . To derive single values, the results from simulations have been averaged along the extraction line for the reach that equals the module extension (i.e. the distance between the axis of the devices along the first line).

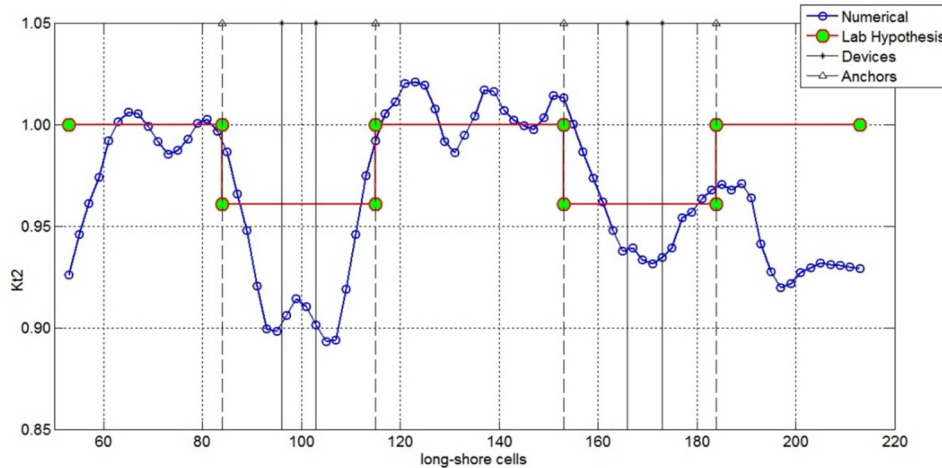


Figure 6. K_T behind the first farm line for the WS n.2; in red: laboratory hypothesis; in blue: numerical results.

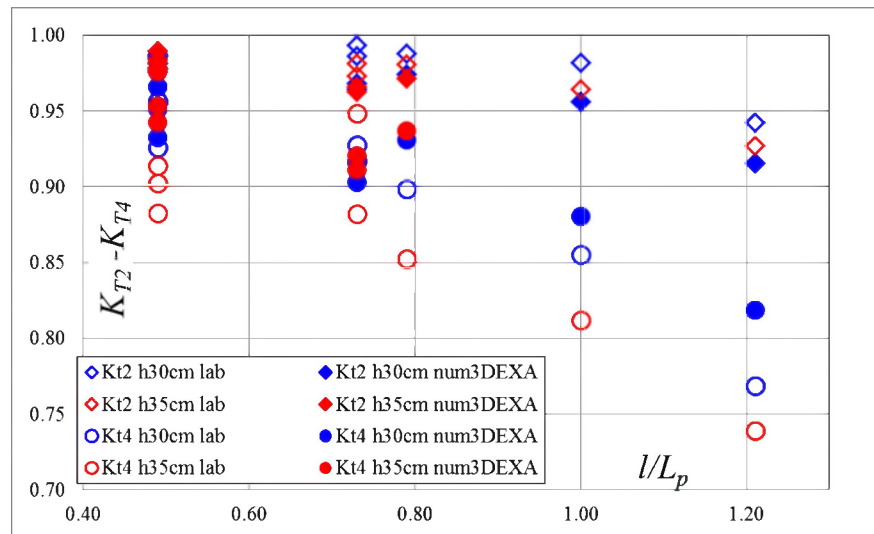


Figure 7. Average K_T behind the first farm line (K_{T2}) and the whole farm (K_{T4}) from the laboratory and the numerical tests.

By means of numerical simulations it is possible to obtain 2D maps, in addition to local values only. Figure 8 reports as an example the disturbance coefficient, i.e. the ratio between the local H_S and the incident H_S at the wave-maker. Values from green to blue denote areas where the devices are effective in reducing wave height, i.e. device wake extension. Values from yellow to red denote areas where the local wave height is greater than the target; it can be specifically noticed wave reflection in front of the three devices and the greater wave heights at the gap induced by the interaction of the devices placed in the first line. The wakes behind the first two devices have an orientation of about 30° with respect to the direction of wave propagation and show an extension greater than the distance between the anchors. The disturbance coefficient varies in the range 0.90-0.98 in the gap and 0.86-0.94 in the wake of the third device.

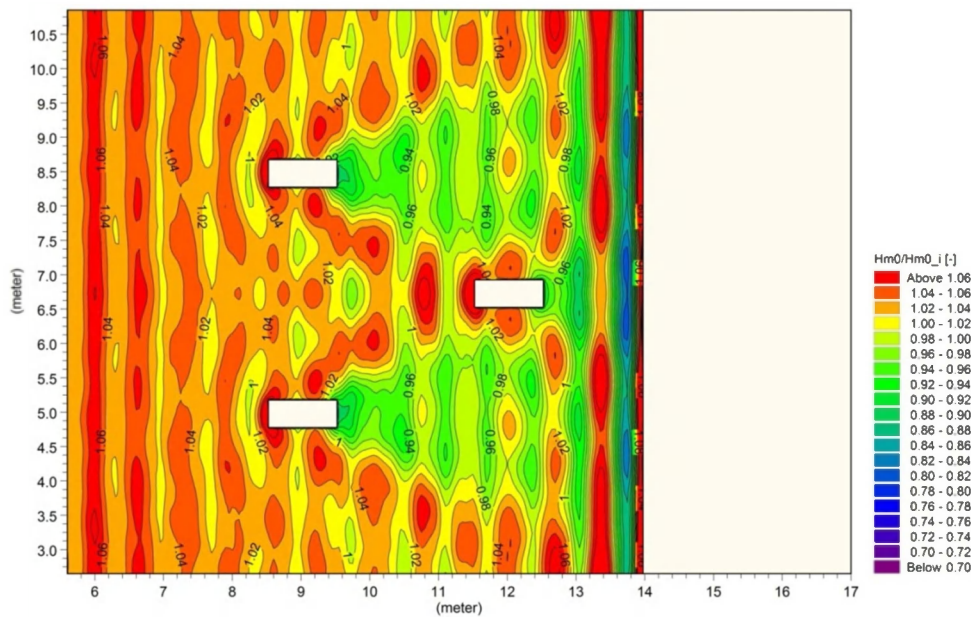


Figure 8. Disturbance coefficient derived from the numerical simulation for the staggered wave farm configuration, after 5 minutes of simulation.

4- NUMERICAL EXTENSION OF THE DATABASE

Numerical simulations allow to analyse additional configurations at lower costs than experiments; therefore this contribution investigates the influence of selected design parameters, such as the device alignment and mutual distance. To investigate both the influence of a change in wave height and wave period the numerical tests were carried out for Ws 4-5-7, at 0.30m as water depth.

4.1- Alignment

The second configuration is an aligned configuration with four devices, two for each line (see Fig. 9). The distance between the farm lines is kept constant. Furthermore, to compare the results with the initial configuration, the same 27 WGs are used, with the addition of other 3 WGs (WGs 22a-23a-24a) behind the new back device.

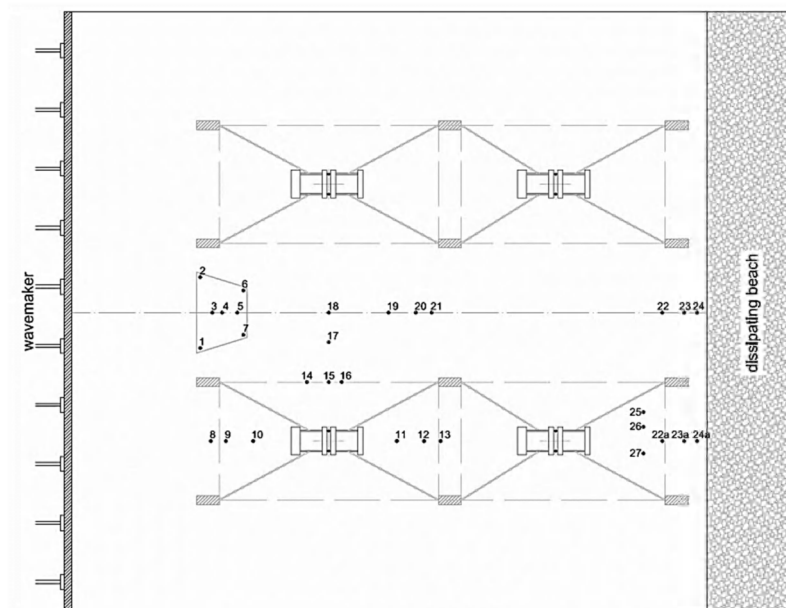


Figure 9. Aligned configuration with four devices (two for each line) with the same 27 WGs, and 3 further WGs (22a-23a-24a) behind the new back device.

As expected, the addition of a fourth device in the second line leads to variation of H_S only for the WGs between the devices and the beach, in fact due to the absence/presence of the device H_S respectively increases at the WGs 22-23-24 and decreases at the WGs 25-26-27 (see Fig. 10).

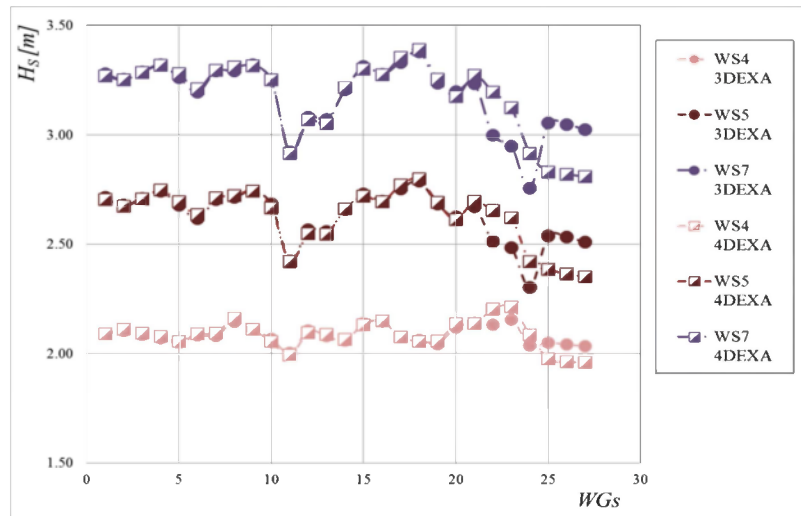


Figure 10. Numerical H_S for all the 27 WGs, derived from the staggered (circles) and aligned (squares) wave farm configuration.

From the 2D map of the disturbance coefficient (see Fig. 11) it is seen that the back devices fall completely in the wake of the first line and the wakes of the second line are affected by wave reflection from the beach. Therefore the values of H_S in front of the back devices and also behind them (and in turns the values of K_{T3}) are lower than in the staggered case. However in the aligned configuration the free area is globally wider and therefore K_{T4} is not so reduced with respect to the staggered configuration (see Tab. 4). If one considers the combined application for energy production, the wave energy available in front of the second farm line is clearly lower.

The disturbance coefficient at the gap and in the wakes of the back devices is in the range 0.90-0.98 and 0.78-0.90 respectively.

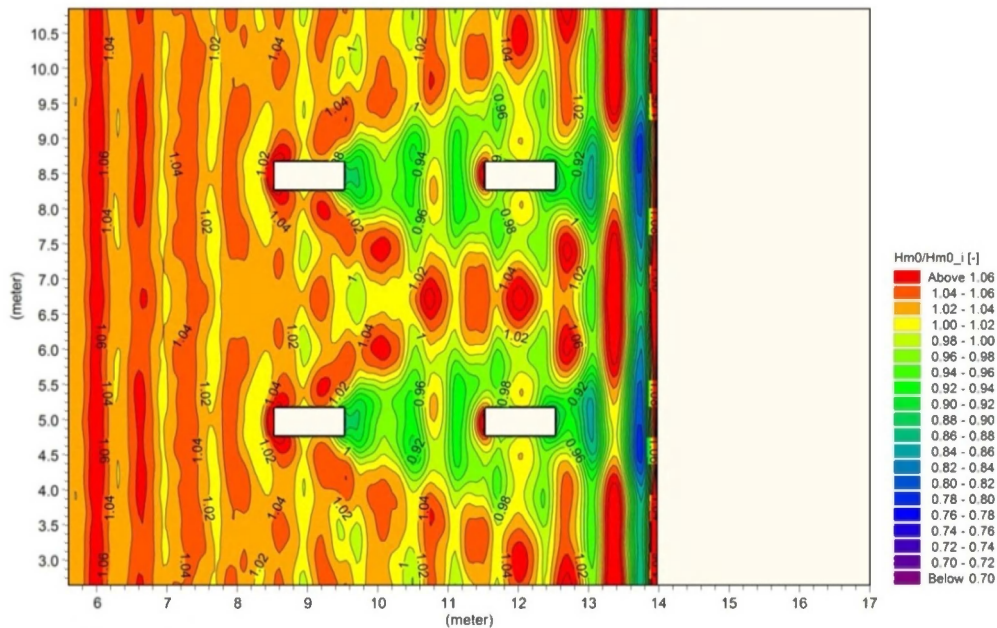


Figure 11. Disturbance coefficient derived from the numerical simulation for the aligned wave farm configuration, after 5 minutes of simulation.

The back device is more affected by the wake of the front devices (see Fig. 14) than in the initial configuration, leading to a lower H_S in front of the back device and therefore a lower H_S behind it. Furthermore, it can be also observed again the reduction of H_S in the gap (especially in long-shore direction). The disturbance coefficient at the gap and in the wakes of the third device is in the range 0.90-1.02 and 0.82-0.92 respectively.

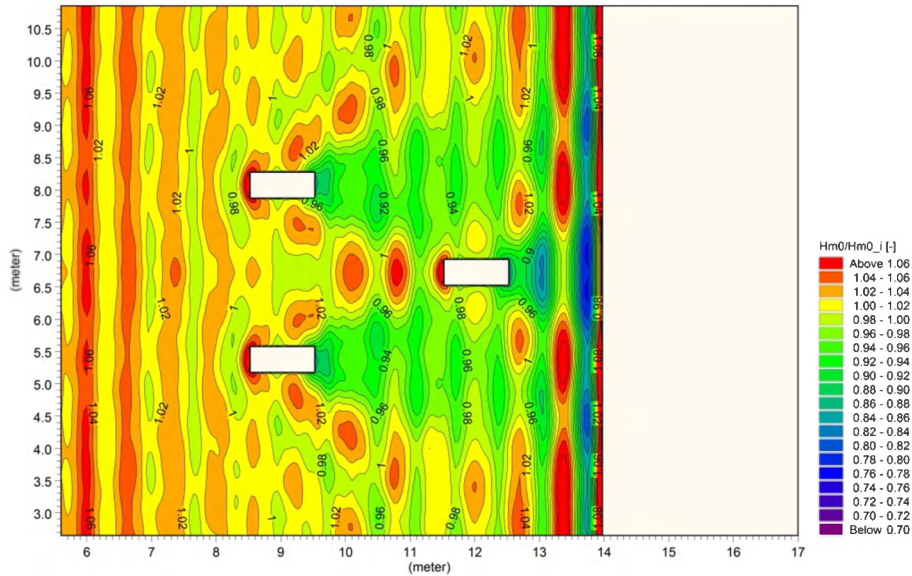


Figure 14. Disturbance coefficient derived from the numerical simulation for the staggered configuration with a gap width of $6b$, after 5 minutes of simulation.

4.3- Optimal configuration

The selection of the best configuration depends on the contemporary achievement of a good level of wave reduction for coastal protection and a sufficient level of wave energy still available at the second line for energy production purposes. The combination of these results leads to a feasible farm installation.

Figures 15 and 16 report the numerical values of the H_S extracted along two long-shore lines, respectively behind the first wave farm line and behind the whole farm for the three configurations described above, e.g. for the WS 5.

From figure 15 it can be derived that the values of H_S are -as expected- the same in case of the 4 DEXA and in case of 3 DEXA with wider gap, whereas for 3 DEXA with narrower gap the values of H_S at the gap are globally lower. This may suggest that an additional reduction of the gap width would lead to stronger wave interactions and greater wave reduction. However this further reduction should account for mooring design also.

Behind the whole farm (see Fig. 16) the differences among the values of H_S for the 3 DEXA cases are small: as in figure 15 the values are lower at the gap for the configuration where the devices are closer. In case of 4 DEXA there is a relevant reduction of H_S only behind the devices.

Based on the limited number of tests carried out and on the model limitations (missing representation of the device motions) it can be concluded (see Tab. 4) that the configuration with 3 DEXA leads to lower wave transmission behind the whole farm and greater wave energy available behind the first line of devices. The performance with three devices in case of narrower gap is not particularly enhanced but is at least constant – leading overall to the best configuration since it also minimizes the marine space required for the installation.

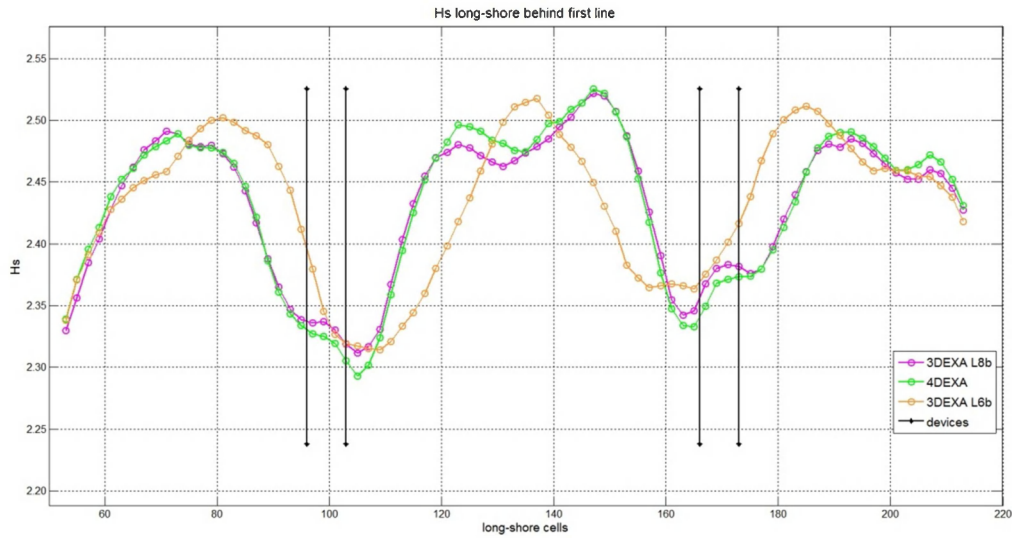


Figure 15. Numerical H_s in long-shore direction, for the WS 5, derived behind the first farm line from the three configurations: staggered with a gap wide $8b$ (purple), aligned (green) and staggered with a gap wide $6b$ (orange). The black lines represent the two first line devices positions.

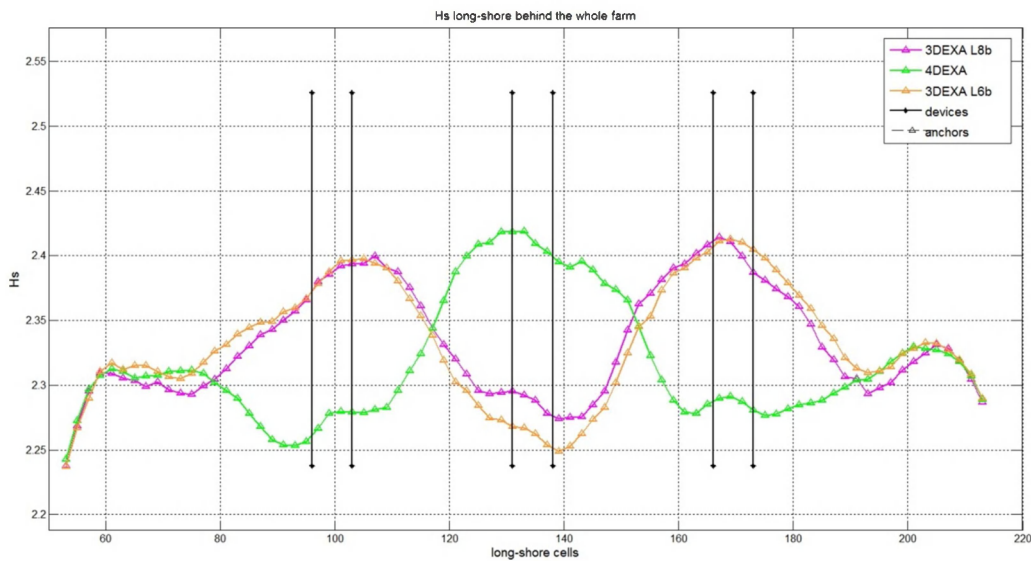


Figure 16. Numerical H_s in long-shore direction, for the WS 5, derived behind the whole farm line from the three configurations: staggered with a gap wide $8b$ (purple), aligned (green) and staggered with a gap wide $6b$ (orange). The black lines represent the two first line devices positions and the third back device.

Table 4. Comparison of the K_{T2} and for K_{T4} for the laboratory and numerical configurations, where 3DEXA L8b means the initial configuration, 4DEXA the aligned, 3DEXA L6b the staggered with the reduction of the gap width.

WS	K_{T2}				K_{T4}			
	LAB	3DEXA L8b	4DEXA	3DEXA L6b	LAB	3DEXA L8b	4DEXA	3DEXA L6b
4	0.99	0.99	0.98	0.98	0.96	0.97	0.97	0.96
5	0.99	0.97	0.96	0.96	0.93	0.92	0.93	0.93
7	0.99	0.96	0.96	0.95	0.92	0.90	0.92	0.92

5- CONCLUSION

The paper presents the physical and numerical study performed on a wave farm of devices of the WAB type named DEXA. The tested module is composed by two devices along the first farm line and one along the second line placed in a staggered position.

The physical tests have been carried out in the directional deep wave basin of the Hydraulics and Coastal Engineering Laboratory at Aalborg University, DK, while the numerical tests have been done with the code MIKE 21 BW developed by DHI Water & Environment & Health.

As regards the laboratory data, each device leads to $K_T > 0.85$ - therefore the placement in farms is required for combining coastal protection and energy production.

K_T depends on $1/L_p$ - therefore the device design can be optimised based on the local wave climate. Water depth variations at installation show a modest effect on the induced hydrodynamics - therefore these devices can face sea level rise. In wave farms, non-linear hydrodynamic interactions play a significant role in reducing K_T (in fact K_{Td} is in the range 0.74 - 0.90).

In the numerical modelling the devices are represented by means of porous layers (i.e. fixed porous piles with rectangular cross section) and therefore the simulations do not capture the hydrodynamic effects of device motions. The numerical tool:

- can represent only the overall reduction of the incident wave height if properly calibrated, e.g. based on the experimental values of wave transmission and reflection induced by the devices. Results of the calibration process specifically led to the conclusion that the porous factor is a key modelling parameter and that an accurate representation of the dissipation at the beach is essential;
- may be used for a parametric analysis of different layouts.

Two additional configurations have been analysed, a staggered layout with a reduced gap width between the devices of the first farm line and an aligned configuration with four devices and constant gap width. Based on numerical results in terms of wave disturbance coefficient and wave transmission behind the farm lines, the best configuration for both coastal protection and energy production is a staggered layout where the long-shore distance among the devices should be kept the minimum that allows the moored devices to freely move, in order to benefit from wake effects for hydrodynamic purposes and maximize device density for marine spatial planning requirements.

ACKNOWLEDGMENTS

The support of the European Commission through Contract 244104 THESEUS ("Innovative technologies for safer European coasts in a changing climate"), FP7.2009-1 Large Integrated Project, is gratefully acknowledged.

REFERENCES

- Angelelli, E., Zanuttigh, B. and Kofoed, J.P. 2012. Numerical modelling of the hydrodynamics around the farm of Wave Activated Bodies (WAB), 4th International Conference on Ocean Energy, October, Dublin
- Beels, C., Troch, P., De Visch, K., Kofoed, J.P. and De Backer, G. 2010. Application of the time-dependent mild-slope equations for the simulation of wake effects in the lee of a farm of Wave Dragon wave energy converters, *Renewable Energy*, Volume 35, Issue 8, August 2010, Pages 1644-1661
- Cruz, J., Sykes, R., Siddorn P. and Eatock Taylor, R. 2009. Wave Farm Design: Preliminary Studies on the Influences of Wave Climate, Array Layout and Farm Control. Proc. EWTEC 2009, Uppsala, Sweden, [http://www.see.ed.ac.uk/~shs/Wave%20Energy/EWTEC%202009/EWTEC%202009%20\(D\)/papers/218.pdf](http://www.see.ed.ac.uk/~shs/Wave%20Energy/EWTEC%202009/EWTEC%202009%20(D)/papers/218.pdf)
- DHI. 2008. MIKE21 Boussinesq waves module - scientific documentation
- DHI. 2008. MIKE21 Boussinesq waves module - User guide.
- Kofoed, J.P. 2009. Hydraulic evaluation of the DEXA wave energy converter. DCE Contract Report No. 57. Dep. of Civil Eng., Aalborg University, Apr. 2009.
- Madsen, P.A. and Sørensen, O.R. 1992. A new form of the Boussinesq equations with improved linear dispersion characteristics. Part 2: A slowly-varying Bathymetry. *Coastal Eng.* 18, 183-204.
- Nicholls R. J., de la Vega-Leinert A C., (Guest Editors) 2008. Implications of sea-level rise for Europe's coasts. *Journal of Coastal Research*, 24 (2), 285-442.

- Palha A., Mendes, L., Conceiç, J.F., Brito-Melo, A. and Sarmiento, A. 2010. The impact of wave energy farms in the shoreline wave climate: Portuguese pilot zone case study using Pelamis energy wave devices. *Renewable Energy* 35, 62–77
- Wheeler, R.L. 2001. Sir Christopher Sydney Cockerell, C.B.E., R.D.I. 4 June 1910 -- 1 June 1999: Elected F.R.S. 1986. *Biographical Memoirs of Fellows of the Royal Society* 47: 67.
- Zanuttigh, B. 2011. Coastal flood protection: what perspective in a changing climate? The THESEUS approach, *Environmental Science and Policy*, 14, 845 – 863.
- Zanuttigh, B., Angelelli, E., Castagnetti, M., Kofoed, J.P. and Clausen, L. 2011. The Wave Field around DEXA Devices and Implications for Coastal Protection. *Control. Proc. 9th EWTEC 2011*, Southampton, UK